FEEG2001 Semester 2 Design Report

Fixed Wing UAV Group 6

March 12, 2018

Harry Hancock
hceh1g15@soton.ac.uk
ID: 27573877

George Shaw
gas1g15@soton.ac.uk
ID: 27742628

Saul Skirvin
ss19g15@soton.ac.uk
ID: 27849295

Gavin Vales
gllv1g15@soton.ac.uk
ID: 27733408

Leszek Wierzchleyski
lw13g15@soton.ac.uk
ID: 27855538

Contents

1 Details of Final Design

1.1 Final Design Selection

1.1.1 Wing Planform

In light of the Wing Design Team's feedback on their concept selection in the Conceptual Design Report, the process of wing planform selection was changed to fall in line with a more engineering appropriate approach to concept selection. The set of wing requirements produced in the conceptual design report was thus changed to the following (aside from the design constraints outlined in the project brief):

	1	2	3	4	5	6	7	8	Normalised Score	Weighting
1	-	0	0	1	1	1	0	1	5	0.139
2	1	-	1	1	1	0	1	1	7	0.194
3	1	0	-	1	1	0	0	0	4	0.111
4	0	0	0	-	1	0	1	0	3	0.083
5	0	0	0	0	-	0	0	0	1	0.028
6	0	1	1	1	1	-	0	1	6	0.167
7	1	0	1	0	1	1	-	0	5	0.139
8	0	0	1	1	1	0	1	-	5	0.139

Figure 1.1: Binary weighting matrix produced for the wing's requirements

1. Low Mass
2. Good Structural integrity
3. Easy Assembly
4. Easy Maintenance
5. Low Cost Materials
6. Simple Manufacturing Method
7. Reliability
8. Sufficient thickness for control surface & HLD mechanisms

No.	Design Variables	Ranked Importance
1	Wing Loading	2
2	Drag Force	4
3	Lift Force	3
4	High Span-wise Strength	1
5	Aspect Ratio	5

No.	Planform Concepts	Ranked Importance
1	Elliptical	3
2	Rectangular	1
3	Tapered (non-swept)	2
4	Tapered (swept back)	4
5	Multiple wing planes	5

No.	Manufacturing Methods	Ranked Importance
1	Wire-Cut Foam	1
2	Laser-Cut Skeletal Wooden Frame	2

These requirements were weighted against each other using a simple binary weighting matrix, seen in Figure 1.1 and were then mapped against the design variables shown below, in a QFD analysis, to find which design variable applied the most to the wing requirements. The wing requirements were then mapped against the 5 main wing planform concepts, shown below, produced in the conceptual design report in another QFD analysis.

A final QFD analysis was carried out to determine which of the manufacturing methods discussed in the conceptual design report was viable.

The resulting QFD tables from these analyses can be found in Figures A.1, A.2 & A.3 as appendices. Design Variable [1] was introduced after the interim design review after learning of the effect of an aircraft's wing loading on its controllability.

These QFD analyses became incredibly useful after the interim design review when it was learned that the wing design process had some errors (see **Section 1.1.3**), and thus limited time was available for optimisation of the wing planform.

Obviously, the most important design variables were the wing loading and the wing's span-wise strength, as they affect how easy the UAV will be to control, and whether or not the wing will be able to handle the lift force that it produces.

The wing's drag is not of utmost importance, as long as it is designed sensibly so as not to have a profile that produces extreme amounts of drag. However, the planform optimisation process will still try to minimise the wing's drag as much as possible as a learning exercise. Also, since the wing will not be experiencing excessively high Reynold's numbers, there is no need for high speed features, like a high sweep angle, to reduce the wing's pressure drag. Thus, the wing's planform will tend towards the more conventional high span, small chord, shape, resulting in similar aspect ratios for all the wing concepts that are produced.

A multiple wing plane configuration concept ranked very low, mainly due to the fact that the wing needs to be designed *and* manufactured in as little time as possible, and with as little resources as possible, to ensure that the engineering design and manufacture centre's materials are not wasted. The tapered (swept-back) planform concept was also of little importance since this type of wing is primarily used to reduce a wing's compressibility drag at low transonic velocities, and, as explained previously, the UAV will not be operated at excessively high speeds. Furthermore, to allow the wing to fit within the 900x250x250mm box constraints, the sweep angle would have to be small, negating any aerodynamic benefits anyway. Again, the wing's aerodynamic efficiency is not of utmost importance, explaining why the elliptical and tapered wing planform concepts were not top ranking.

This QFD analysis whittled down the choice of concepts to the rectangular, elliptical and tapered (non-swept) concepts. As detailed in the conceptual design report, the two main things considered in the concept choice were their cost effectiveness (with respect to ease of manufacture), and their aerodynamic efficiency. With this in mind, the tapered planform was chosen as it offered a a simple trade-off between aerodynamic efficiency and cost effectiveness. The taper ratio would not be too great however,to allow the wing to have sufficient thickness along its span for servos, and also to keep the wing's centre of gravity close to its quarter chord point, which is an important constraint as it keeps the UAV's CG within its static margin (stability condition for trimmed flight). The CG position can of course be modified further by adjusting the position of the electronics placed in the fuselage. This planform would also mean fewer materials would be required for manufacture than a rectangular wing, no matter which of the manufacturing processes are chosen.

Also mentioned in the conceptual design report was the original plan to make the wing as a skeletal wooden frame, but the time constraints after the interim design review meant that a final QFD analysis had to be done to make sure that this manufacturing method was still viable. Thus, it was decided to cut the wing out of foam, not only to deal with the time constraints, but also because of the planform optimisation process used (**Section 1.2**).

1.1.2 High Lift Device/Control Surface Type & Mechanism

We started with 4 quality function deployment (QFD) tables in order to find the most appropriate flaps, ailerons, slats and materials for our project. The design requirements for these QFD tables were based on relative importance in a design matrix (see conceptual design report). From the QFD tables we created 3 concepts for high lift device configuration:

- A simple design consisting of plain flaps and Frise ailerons 3D printed from ABS resin with no slats
- A design which focused on generating maximum lift consisting of Fowler Flaps, Frise ailerons and sealed slats which would all be cut out foam.
- A compromised design with the objective of producing maximum lift with the simplest production which consists of plain flaps, Frise ailerons and sealed slats which would all be 3D printed from ABS resin

We decided very early on that the second concept (high lifting) would not be the most appropriate option as the increase in lift would not justify the risk of using the very complicated Fowler flaps (Figure 1.2). These Fowler flaps would require a greater number of moving parts than plain flaps and more moving parts increase the chances of failure. Furthermore, the mechanism of a Fowler flap involves parts running along tracks which opens up the opportunity for failure, which is not possible for a plain flap which only requires a hinge. For these reasons, we ruled out this design.

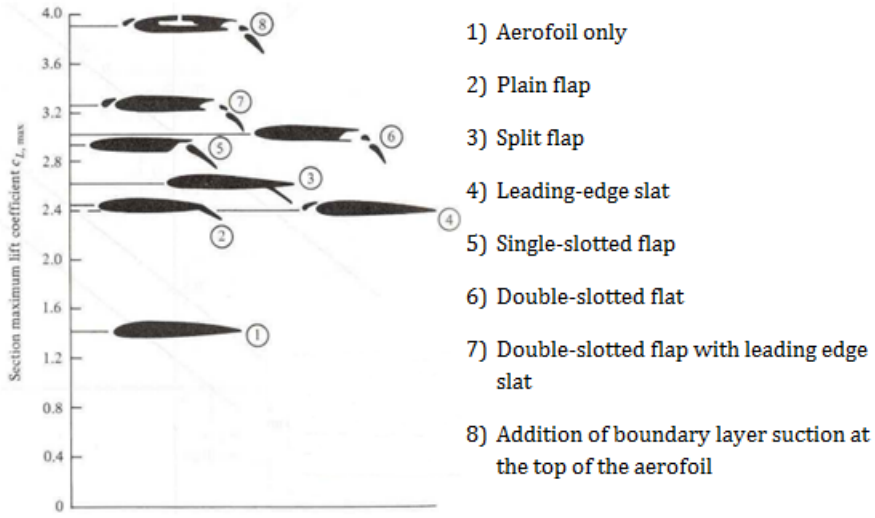

Figure 1.2: Typical values of aerofoil max. C_L for various types of high lift devices [1]

In all three concepts, we had decided to use Frise ailerons as these scored the highest on the aileron QFD table. However, following a lecture on flight mechanics in which ailerons were discussed, we decided that it would be more appropriate for us to use differential ailerons. This is because Frise ailerons utilise aerodynamic forces over the wing in order to alleviate adverse yaw which would require a lengthy process in order to design the perfect flap profile. We didn't have the time to go through all of the iterations that would be required and it made sense to use differential ailerons. Differential ailerons alleviate adverse yaw by being set to different angles which is simple to set on an Arduino (Figure 1.3).

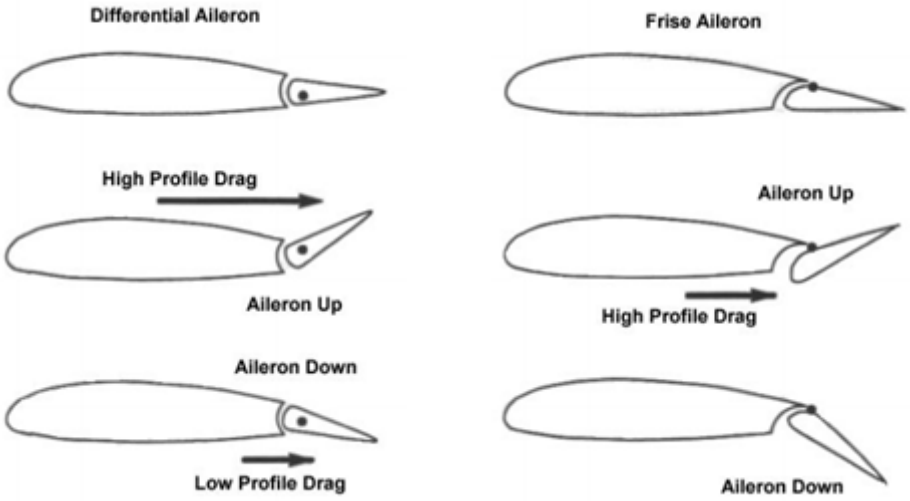

Figure 1.3: Comparison between differential and Frise ailerons in the mechanisms of alleviating adverse yaw [3]

We had proposed in both of the remaining concepts that the parts would be 3D printed from ABS resin, because ABS resin is stronger and more structurally sound than foam. However, after the interim design review, we decided that it was more important to save weight because two Arduinos were to be used. Therefore, we decided that the high lift devices would be cut out of foam.

The only difference between the two designs left in contention, the simple design and the compromised design, was the inclusion of sealed slats. Ultimately, we had to determine whether the lift provided by the slats justified the consequences. The consequences were the additional computing power required to operate them, the additional weight added by the mechanisms and the risk of them getting jammed at an undesirable extension which would have a detrimental effect on the aerodynamics of the wing. The flow simulations that we ran in SolidWorks showed us that the inclusion of slats did have a considerable effect on the lift generated by the wing. We also knew that we could solve the potential jamming problem using silicone gel lubricant. However, ultimately, we decided that the addition of slats would not be the best decision due to the additional computing power required and the large increase in the complexity of the design, both mechanically and in terms of the computer code. An additional factor in the rejection of slats was the fact that the design of the final wing took longer than expected. This left us with less time to design and optimise the slat in order to meet the deadline to get it cut from foam. This decision was vindicated as the simulations demonstrated that it was possible to generate sufficient lift without the slats. The design would also be cheaper and lighter without slats.

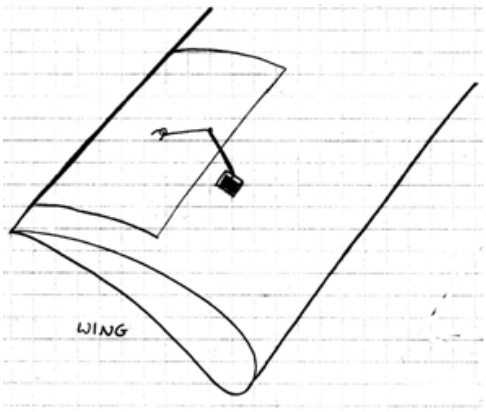

Figure 1.4: A view of the wing including the servo and mechanism for deploying the high lift device

From these analysis processes, we decided that the high lift devices would consist of plain flaps and differential ailerons cut from foam.

The deployment mechanism for both the aileron and the flap involves thin metal beams with a hinge connecting them (Figure 1.4). The servo will be mounted on the wing in the middle of the flap or aileron. A hook would be attached to the flap or aileron to attach it to the beam. A hinge made from a similar thin metal beam will run through the high lift device in order to allow it to pivot.

This mechanism was chosen because our other concept was only possible if the high lift devices were going to be 3D printed. The light weight of the beams and the simplicity of the hinge make this configuration perfect for the final design.

1.1.3 Wing-tip Devices

Originally it was intended to attach one of 3 types of tip devices to the wing. However, during the interim design review, we learned of one main fault with our wing design process: we optimised our wing's aerofoil, before optimising its planform (for structural rigidity etc.). Thus, there was limited time available after the interim design review to allow detailed analysis of the wing planform and aerofoil, *as well as* the tip devices, in time for foam cutting by week 8.

1.2 Analyses Performed

1.2.1 Sizing Wing Planform

	Lower Bounds	Upper Bounds
Semi-Span [m]	0.6	0.9
Root Chord [m]	0.15	0.25
Taper Ratio	0.6	1.0
Max. Wing Thick. [% chord]	15	25

Table 1.1: Wing PlayPen Parameter Bound Set 1 [BS1]

Weighting Combination	Total C_D	Wing Mass [kg]
20;1	0.01649	0.4512
10;1	0.01703	0.4376
1;1	0.01703	0.4376
1;10	0.01702	0.4337
1;20	0.01706	0.4376

Table 1.2: Results from investigation of Drag;Mass weighting combination

	Lower Bounds	Upper Bounds
Semi-Span [m]	0.75	0.9
Root Chord [m]	0.15	0.25
Taper Ratio	0.75	1.0
Max. Wing Thick. [% chord]	15	21

Table 1.3: Wing PlayPen Parameter Bound Set 2 [BS2]

	Lower Bounds	Upper Bounds
Semi-Span [m]	0.75	0.9
Root Chord [m]	0.15	0.25
Taper Ratio	0.75	0.95
Max. Wing Thick. [% chord]	16	19

Table 1.4: Wing PlayPen Parameter Bound Set 3 [BS3]

Due to the time constraints, as mentioned in **Section 1.1**, a fairly short and easy to use wing sizing program was required. This came in the form of the UAV Wing Design Playpen, which optimises a wing planform, assuming the wing is to be made out of foam. Table 1.1 shows the first set of bounds used for the working parameters in the playpen. The ranges were chosen to be big enough to allow the program to converge on suitable values, but small enough so that it can converge on suitable values in fewer iterations.

A total of 5 Drag;Mass weighting combinations, seen in Table 1.2, were investigated with these bounds, before finding viable solutions for the wing parameters. Each combination was investigated by optimising the total C_D, while trying to produce similar wing masses for each weighting combination, so that we could see how the weightings affect the C_D optimisation. Thus, the 20;1 weighting combination was chosen as it produced the lowest total C_D.

The optimisation process was then carried out normally, minimising both wing mass & C_D, using the same bounds (seen in Table 1.1), and then for smaller bound ranges, seen in Tables 1.3 & 1.4. The results from each of these optimisation sets are in Table 1.5. Values for each parameter are rounded to 4 significant figures. As you can see, Bound Set 2 produced a desirable Min. C_D and Min. Wing Mass combination.

Out of the bounds investigated, its C_D and Wing Mass values were a trade-off between the low Wing Mass from Bound Set 1, and the low C_D from Bound Set 3. Note that the calculated Axial Bending Stress and Cruise Wing Loading didn't exceed their set limits during any of these cases. The final values of the wing's semi-span, root chord, taper ratio and maximum thickness used in the x-foil analyses were 890mm, 190mm, 0.9 & 16%, respectively.

Parameter	BS1	BS2	BS3
Wing Mass [kg]	0.3979	0.4077	0.4231
C_D	0.01733	0.01659	0.01639
Semi-Span [m]	0.8813	0.8906	0.8883
Root Chord [m]	0.2078	0.1938	0.2156
Taper Ratio	0.7938	0.9336	0.8188
Max. Wing Thick. [% chord]	18.28	16.78	17.08

Table 1.5: The final parameter results from the the UAV Wing Design PlayPen for each parameter bound set

Screen shots of the rest of the starting parameters used in the Aerodynamics and Structures spreadsheets can be found in Figures B.1 & B.2. The 'Fuselage (and all else)' mass used was taken as a maximum, and was calculated using the data from this GDP's FAQ. The estimated Oswald span efficiency was chosen to be roughly at the lower end of its recommended range, given in the Aerodynamics spreadsheet, and the Maximum Load Factor chosen to be at the upper end of its recommended range, to ensure the wing is structurally sound. The upper Cruise Wing Load limit was calculated online for a constant chord wing with the maximum possible dimensions (900mm semi-span & 250mm chord) to force the program to produce a planform with as low a wing loading as possible. A 100m altitude is roughly the maximum range of the transmitter, and the $12.5ms^{-1}$ flight velocity is the take-off velocity stated in the Project FAQ. The address of the website used to calculate the cruise wing loading limit is as follows:

`http://www.flyingsites.co.uk/downloads/wingloadcalc.htm`

In the structures spreadsheet, the spar type and dimensions are of those used in the previous year's UAVs, made from carbon fibre. Originally, it was intended to equip the wing with slats, as well as flaps, so the structures spreadsheet shows 6 servos (one each for 2 ailerons, 2 flaps & 2 slats). But, as will be explained later in this section, it was decided that slats were not feasible, while the wing was being manufactured. Thus, the the wing may be oversized. The position of the maximum wing thickness was set to 25% of the chord to ensure that the CG position constraint is roughly adhered to.

Some Drawbacks of this Analysis

One main drawback to this analysis was due to the time constraints, and the fact that this was the first time this group had carried out this analysis. In other words, there was no similar previous UAV wing from which more accurate values for the starting constraints (in Figures B.1 & B.2) could be obtained. As a result, the most inaccurate estimates occurred for the Oswald span efficiency, which varies with the wing's geometry (so was assumed to be between 0.78 & 0.97) and maximum load factor, as the strength of gusts that the UAV will experience, and the load factor that it will experience at take-off (and landing), cannot be very well predicted.

A second drawback to the above analysis arises since a more thorough investigation of the consistency of each PlayPen analysis was not carried out i.e. to see whether or not it gives the same set of optimised wing parameters after several iterations using the same starting constraints. This was done only a few times using Bound Set 1, which did produce the same results each iteration, but is not completely conclusive evidence of the reliability of each analysis.

1.2.2 Aerofoil Optimisation

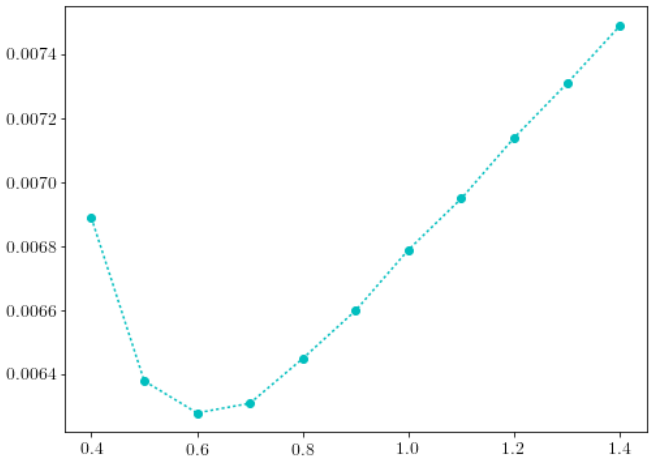

Figure 1.5: Plot of C_D vs. Upper Control Point weighting, with 0.5 lower control point weighting

As noted in our interim design review, it was decided to optimise our own aerofoil using code created in our Part 1 Semester 2 Computing project and the 2D XFoil software. Optimisation began by changing the weighting on the upper control point of a normalized bezier aerofoil to find which gives the minimum sectional C_D (Figure 1.5). Figure C.2 illustrates the aerofoil.

The weighting of the lower control point was chosen to ensure that the aerofoil would have sufficient camber (produce a sufficient lift coefficient) at any upper control point weighting. The lower and upper control points are co-linear with the 5% chord position, to keep the maximum thickness and centre of area position close to the quarter chord.

For a given uniform free-flow velocity, as an aerofoil's camber increases, so does the speed of the fluid over its upper surface. This advances the onset of pressure drag over the aerofoil as the flow separation point on the aerofoil's upper surface moves closer to the leading edge. This produces the trend seen in Figure 1.5.

As you can see from Figure 1.5, the optimum upper weight was 0.6, producing an aerofoil with a C_d of 0.00628. However, this aerofoil's thickness was much smaller than that produced from the Play Pen, so would definitely not be able to house the servos or the spar. The upper control point weighting thus had to be increased to 1.0, 1.2 and then 1.4, to produce an aerofoil with the appropriate properties. Obviously, the the lower control point weighting had to be increased to get the correct aerofoil thickness, but overall, there was only a maximum increase in the aerofoil's C_D by about 20% (from the optimum). The properties of these aerofoils are shown in Table 1.6.

Aerofoils 5, 6 & 7 were the final aerofoils produced from this part of the optimisation process (shown in Figures C.3, C.4, C.5, respectively) and underwent further optimisation in the 3D XFoil software.

'foil No.	Upper Weight	Lower Weight	C_d	Max. Thick. [%chord]	Max. Thick. Position [%chord]
1	0.6	0.5	6.28E-3	11.72	29
2	1.0	0.5	6.79E-3	13.93	27
3	1.2	0.5	7.14E-3	14.76	26
4	1.4	0.5	7.49E-3	15.47	25
5	1.0	1.4	7.52E-3	15.81	25
6	1.2	1.0	7.52E-3	16.00	25
7	1.4	0.7	7.63E-3	16.04	25

Table 1.6: Properties of Bezier aerofoils produced using the python code

Comments on the Python Code

The python code makes the aerofoil by joining together two rational cubic Bezier splines, one each for the the upper and lower surface of the aerofoil, via a control point at the leading of the. This aerofoil is converted into a set of 201 *(x,y)* coordinates, which are placed into a `.dat` file, and is then analysed in XFoil 6.99 using the inputs in Figure C.1. The Reynold's number & Mach number values were calculated assuming the fluid was standard air, and the flow speed was 12.5 m/s.

The value of C_D was then extracted from the outputted polar. Changing the weighting on the upper control point (at (0.05, 0.20)), a different aerofoil can be produced, which can also be analysed.

This process is repeated for a set list of control point weightings, plotting the C_D vs. the value of the upper control point weighting (seen in Figure 1.2).

1.2.3 UAV CG Optimisation

b	0.89	b_T	0.42
c	0.19	c_T	0.1
S	0.1602	S_T	0.042
A	4.944	A_T	4.200
e	0.75	e_T	0.70
$C_{L\alpha}$	4.082	$C_{LT\alpha}$	3.739
$C^*_{L\alpha}$	5.062		

Table 1.7: Values of parameters used to find the UAV's neutral point

This process began by using the equation for an aircraft's static equilibrium CG margin, from [2], to find which of the possible wing positions wrt. the fin, l, shown in Table 1.8, produced a suitable CG margin. The maximum l value lines the wing's root leading edge with the peg-hole (on the fuselage) closest to the fuselage nose, and minimum value ensures the wing's trailing edge doesn't come into contact with the ducted fan's stand. l is decreased by the amount corresponding to the distance between the peg-holes (roughly $15mm$).

The UAV's actual CG, at each wing position, was found in a rather crude manner using SolidWorks' 'Mass Properties' function. The mass of the electronics was simulated by augmenting the electronics tray's mass to $766g$, and then setting the tray's CG to be collinear with the wing's root leading edge, producing a virtual electronics mass that would move with the wing.

l_0 (mm)	l (m)	K	$\frac{C_{LT\alpha}}{C^*_{L\alpha}}$	h_n	CG x-coord (mm)	h
700	0.6775	0.9349	0.7387	0.9406	89.09	0.4949
685	0.6625	0.9142	0.7387	0.9253	88.55	0.4919
670	0.6475	0.8935	0.7387	0.9100	88.01	0.4889
655	0.6325	0.8728	0.7387	0.8947	87.47	0.4859
640	0.6175	0.8521	0.7387	0.8794	86.94	0.4830

Table 1.8: Investigation of the UAV's static margin

The UAV's neutral point (the CG position where an aircraft becomes neutrally stable) was calculated using equation 1 [2].

$$h_n = h_0 + K\frac{C_{LT\alpha}}{C^*_{L\alpha}} \tag{1}$$

for $C_{LT\alpha} = \frac{2\pi A_T e_T}{A_T e_T + 2}$, $C^*_{L\alpha} = C_{L\alpha} + C_{LT\alpha}\frac{S_T}{S}$, $K = \frac{S_T l}{Sc}$, and $C_{L\alpha} = \frac{2\pi Ae}{Ae+2}$. The values of these parameters are shown in Table 1.7.

Since wings with a non-elliptical lift distribution, and which tend to operate at moderate Reynold's numbers (compared to that of high speed passenger airliners), have span efficiencies between 0.7 and 0.85, e_T was set to 0.7 (as the tail-plane has a rectangular planform, with no twist) and e to 0.75 (the wing only has minimal taper).

From Table 1.8, it can be seen that the UAV has its maximum CG margin when $l_0 = 700mm$, and due to the fact that the CG position varies by only about a centimeter over the range of wing positions, it was decided to position the wing at $l_0 = 640$ (i.e. as close to the EDF as possible), to allow the mass of the electronics to be moved as far forward so as to keep the CG of the UAV close to the quarter chord of the main wing. If the CG *can only* get close to the quarter chord, then the large h_n calculated at this wing position ensures that the UAV will still be stable.

Obviously, this rudimentary analysis will be inaccurate: there was no nose in the SolidWorks assembly of the UAV, the mass and CG of the electronics could not be measured soon enough, and the whole UAV's CG will not move . However, it does illustrate whether or not the UAV will be stable.

Unfortunately, we could not perform an XFLR5 stability analysis to find the UAV's lateral and longitudinal modes. The program wasn't able to analyses our custom aerofoil. This may be because the aerofoil wasn't defined with enough points, making its surface too rough.

1.2.4 Mesh Independency [XFLR5]

To achieve mesh independency for the wing analyses, the number of x-panels and y-panels were increased in the plane editor by 10 each time to increase the number of mesh elements. This was done until the C_L and C_D remained the same.

	No. of Mesh Elements													
AoA	494 mesh elements		2574 mesh elements		4214 mesh elements		6254 mesh elements		8694 mesh elements		11534 mesh elements		14774 mesh elements	
-	C_L	C_D	C_L	C_D	C_L	C_D	C_L	C_D	C_L	C_D	C_L	C_D	C_L	C_D
0	0.2	0.001	0.206	0.002	0.206	0.002	0.207	0.002	0.207	0.002	0.208	0.002	0.208	0.002
2	0.371	0.005	0.376	0.005	0.377	0.005	0.377	0.005	0.377	0.005	0.378	0.005	0.378	0.005
4	0.541	0.01	0.545	0.01	0.546	0.01	0.546	0.01	0.546	0.01	0.546	0.01	0.546	0.01
6	0.709	0.017	0.712	0.017	0.713	0.017	0.713	0.017	0.713	0.017	0.713	0.017	0.713	0.017
8	0.874	0.025	0.877	0.026	0.877	0.26	0.878	0.026	0.878	0.026	0.878	0.026	0.878	0.026
10	1.037	0.036	1.039	0.036	1.039	0.037	1.039	0.037	1.04	0.037	1.04	0.037	1.04	0.037

Table 1.9: Mesh Independency Test

1.2.5 Sizing Control Surfaces & High Lift Devices

We performed flow simulation on SolidWorks in order to determine the final configuration high lift devices. For all simulations, the conditions we used were a wind speed of 12.5m/s at an angle of attack of 2^o which are the same as the wing design team used. By attaching one device at a time, starting with a size we determined as being average from research on the internet, we proceeded to find the optimum deployment angle of each device. We started at a deployment angle of 0^o and increased it to 45^o in 5^o increments. We recorded the lift and drag force on the wing and plotted a graph of both in order to determine the optimum angle. Once the angle had been decided, we set the angle of the high lift device to the optimum and the chord-wise length to 5% of the chord. We recorded the lift and drag under the same conditions as before. Then we proceeded to increase the chord-wise length to 35% in 5% increments and plotted a graph as before. We then set the high lift devices to their optimum angle and chord-wise length and proceeded to find the optimum span-wise length. We set the span of the high lift devices to 20% of the span and increased the length in 10% increments to 60%.

In order to determine the optimum span-wise length of each high lift device, we determined that the role of the flaps deemed that they must be at their optimum size. We then made the aileron the maximum size with the space remaining.

Aileron tip is 50mm from the wing tip in order to maximise rolling moment but avoid interference from wing tip. Root of flap is set 100mm from the root of the wing in order to avoid interference from the fuselage. Set as close to the wing root as possible in order to minimise rolling moment in the event of the failure of one flap.

1.2.6 HLD Angle Optimisation

Having determined the optimum size of the high lift devices, we now needed to find the optimum deployment angles. We started with the ailerons, to find the angle that would give us maximum lift, and therefore rolling moment, with minimum drag. We did this in SolidWorks and set the angle to 30^o which was initially found to be optimum. Then we changed the angle in 1^o increments from 26^o to 34^o, recording lift and drag at each point. The optimum was found to be at 32^o which produced $5.065N$ of lift and $0.909N$ of drag. *See Figure D.1*

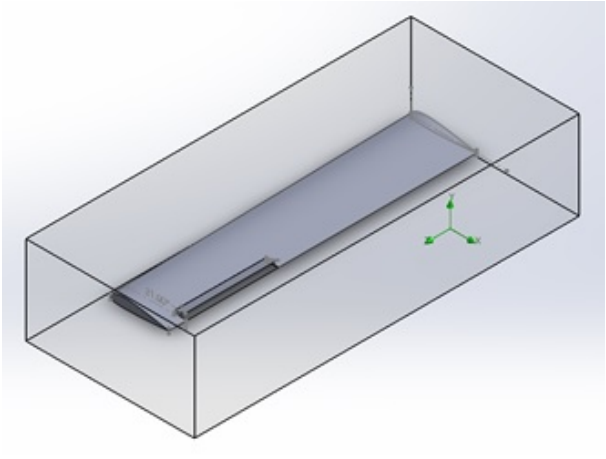

Figure 1.6: An image of the wing on SolidWorks during the flow simulation to find the optimum aileron up angle

The next step was to calculate the aileron up angle which would give us the correct amount of drag in order to combat the effect of adverse yaw. We started at 30^o because it was the angle (to the nearest 5^o) that gave the correct amount of drag in the down direction. It produced $0.772N$ of drag which was too low so we tried 35^o as it was an appropriately sized step. 35^o produced $1.001N$ of drag so we tried 1^o increments from 31^o to 34^o to produce the correct amount of drag. The closest was 33^o which gave $0.901N$. We decided that we should find the angle to the nearest degree as the accuracy of the servo would make it pointless to go to a closer accuracy. *See Figure D.2*

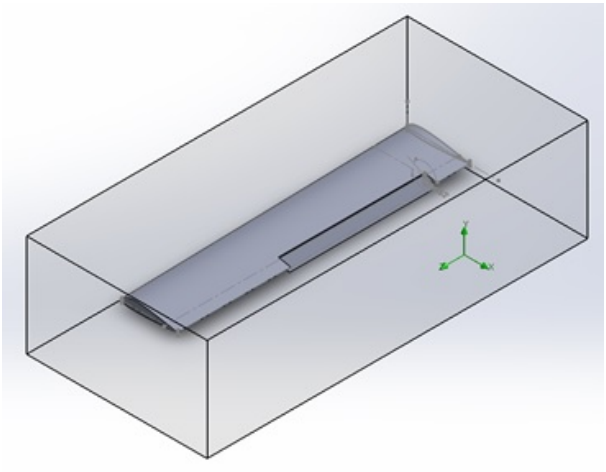

Figure 1.7: An image of the wing on SolidWorks during the flow simulation to find the optimum angle of flap deployment

For the flap angle, we started with a simulation at 30^o which was initially found to be the optimum flap angle to the nearest 5^o. We then ran simulations at 1^o increments from 26^o to 34^o in the same way that we did for the aileron down angle, recording lift and drag at each point. The optimum flap angle was found to be at 33^o where it produced $7.478N$ of lift and $1.126N$ of drag. *See Figure D.3*

1.3 Manufacturing Process

1.3.1 Initial Wing Manufacture

As already mentioned, the wing was cut out of a block of Roofmate Styrofoam roofing insulation. The gaps for the ailerons and HLDs were simply cut out using a Stanley knife, and the sections for the servos were made by heating the head of a flat-head screwdriver, and slowly and carefully melting into the foam (a similar process to that used for cutting out the whole wing).

1.3.2 HLD & Aileron Attachment

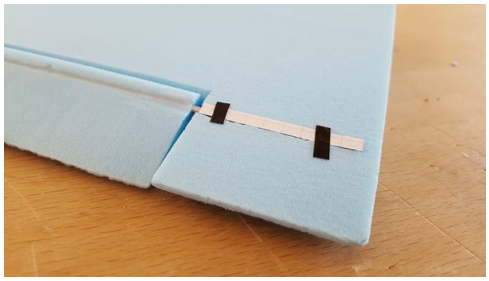

Figure 1.8: An image of the paper strip sitting between the duct tape and the hinge, allowing the hinge to rotate

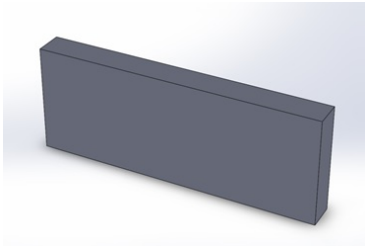

Figure 1.9: A CAD model of the 'rectangle' which is part of the HLD controlling device

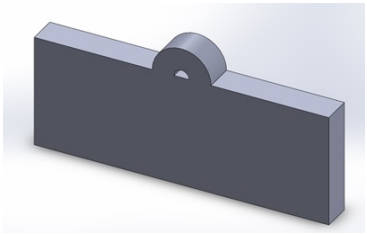

Figure 1.10: A CAD model of the 'briefcase' which is part of the HLD controlling device

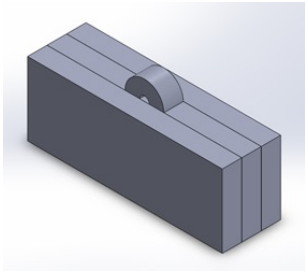

Figure 1.11: A CAD model of the assembly of the HLD controlling device

As previously discussed, we decided to have the HLDs wire cut from foam. In order to do this, we created third angle technical drawing of the flaps and ailerons, from the finalised CAD models in SolidWorks. We then converted these into `.dxf` files and sent them to the technicians for cutting.

In order to attach the HLDs to the wing, the first process required fitting a hinge to them. A coated copper wire needed to be fitted to act as the hinge. We didn't have this hole cut using the wire cutter in case the diameter of the hole would be too small that it melted the foam.

Instead we decided to cut a slot out using a Stanley knife and the slot was refined to the correct size using sandpaper.The same process was used to cut slots in the wings for the hinges to attach to. Once the hinge had been placed in the high lift device, we filled the gap with PVA glue as this would hold the hinge in place and retain the correct HLD profile.

We planned to put PVA glue over the slots in the flaps as well as it would hold the hinge in place but allow it to rotate. This worked on a test piece however when it came to the actual wing, glue slipped down the sides of the hinge and locked it in place, not allowing any rotation.

After safely removing the HLDs from the wing, leaving both intact, we decided that the best method would be to use duct tape to cover the top of the slot as this would allow the hinge to rotate. A small strip of paper was placed underneath the duct tape so that it would not stick to the hinge.

We manufactured a part to fit on the HLDs which would connect to the servos in order to deploy the control surfaces. We intended to 3D print the part however time constraints meant that we had to alter the design in order for it to be laser cut.

The part was going to be glued on the HLD so we needed to ensure there was a large surface area for the glue so that it would not break off. The design consisted of a small loop mounted on top of a larger section. We laser cut 2 different parts: a 'briefcase' and a 'rectangle'. The 'briefcase' was sandwiched in between two 'rectangles' to improve the structural integrity of the device. The parts were stuck together with PVA glue and placed in a clamp while they were drying to ensure they were stuck together in the correct orientation. We used a file and sandpaper to ensure that the surface that would be glued lay completely flat on the HLD and a defect may cause it to break off.

1.4 Final Wing Assembly

Before assembly, we connected the HLD and aileron servos up to the flight computer to centre all the control surfaces. For the ailerons the servo moved through 90 degrees and at 45 degrees this was where the ailerons were flat. The flaps were flat on the wing at 0 degrees then they were deployed through one direction.

To assemble the wing we made a device (Figure 1.12) to keep the wings together at the root so they can be attached to the fuselage. The wires from the servos in the wings were passed through the cut made by the foam cutter when it was cutting the spar hole. This meant the wires could be placed inside the wing in a tight space were the couldn't move during flight. These wires then passed out of the root of the wing and down through the hole in the device and through into the fuselage.

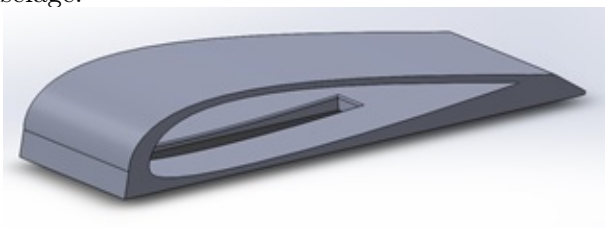

Figure 1.12: The wing attachment device

There is a 10mm carbon fibre spar going through the wing. Inside this main spar, at the root, we put a smaller diameter spar (8mm) through the main spar in a tight fit, to hold the wings together.

On the day of the flight test, to attach the wings to the fuselage, we inserted one wing into the attachment device, inserted the smaller spar and then pushed the other wing into place on the other side of the device. The whole assembly was then placed on top of the fuselage and rubber bands were wrapped around to keep it in place.

2 Flight Controller

The on-board electronics for the UAV were split into four general requirements;

- Manual transmitter control by the pilot.
- Autopilot control, with the ability for the pilot to remotely engage/disengage.
- Flight data recorder, recording a selection of flight data.
- High lift device control, operated remotely through a switch on the transmitter.

The general concept behind the system was to have a master Arduino, which collected data from sensors, manipulated it, made decisions upon it, and adjusted the aileron and elevator angles based upon these decisions. Through the control of these surfaces, the UAV could be flown effectively without the need of pilot input, with the exception to speed control. The master Arduino also had the task of passing data already used to a slave Arduino. This Arduino held a GPS and microSD shield, which collated various parameters of data every second, and wrote them to a data file to be analysed following the flight.

2.1 Pilot/Autopilot Control

To enable the switching between the two flight modes, pilot and autopilot control, a double pole double throw relay was used, in series with a transistor, sourced from the ARDX kits. The signal pulse width from the transmitter was interpreted by the master Arduino, which passed the corresponding high or low signal to the transistor. The relay which was connected to the system with NC (normally closed) being fed signal from the transmitter, NO (normally open) receiving signal from the autopilot system, and COM (output) passing the signal to the control surfaces. A high signal to the transistor would allow power to be received by the relay switch, and the signal passed to COM change from NC to NO or from manual control to autopilot control. A double throw relay was used to allow the use of the signal to two separate control surfaces to be switched by a single switch. The system was connected with the NC signal from the transmitter as a failsafe such that were the Arduino system to fail, or power to the relay lost, the switch would fall back to NC and control of the UAV would be kept by the pilot.

2.2 Autopilot System

When the signal from the transmitter read high, control was switched to the autopilot system, which was programmed to fly the UAV to a set altitude of 20m above the ground, at a heading of due south. The state of the aircraft was determined through the data collected from a BMP085 barometric sensor and an LSM303DHLC accelerometer and magnetometer. Using the (highly reliable) aviation forecast for Southampton Airport, the air pressure could be input into the barometer and an accurate altitude reading taken. Upon setup of the UAV a constant value of ground altitude was stored by the UAV, thus allowing a secondary value of desired altitude of 20m above this ground altitude to be stored. The data from the LSM module could be converted using simple trigonometric functions to output a value for the aircraft heading, and pitch and roll angles of the aircraft. From these three pieces of data, being collected throughout the flight, the decision on what manoeuvre to take could be made and the desired pitch (P) and roll (R) angles decided upon as shown in Table 2.1.

Pitch/Roll	Hard Left	Soft Left	Level	Soft Right	Hard Right
Ascend	$P = 13^o$ $R = -10^o$	$P = 13^o$ $R = -5^o$	$P = 13^o$ $R = -0^o$	$P = 13^o$ $R = 5^o$	$P = 13^o$ $R = 10^o$
Level	$P = 3^o$ $R = -10^o$	$P = 3^o$ $R = -5^o$	$P = 3^o$ $R = 0^o$	$P = 3^o$ $R = 5^o$	$P = 3^o$ $R = 10^o$
Descend	$P = -7^o$ $R = -10^o$	$P = -7^o$ $R = -5^o$	$P = -7^o$ $R = 0^o$	$P = -7^o$ $R = 5^o$	$P = -7^o$ $R = 10^o$

Table 2.1

A hard-banked turn was used when the error in heading was greater than 10^o, below which a smaller bank angle was decided upon until the UAV was heading on a bearing of 180.

From this point, a variable 2-dimensional PID (proportional-integral-derivative) system was used, through advancements made to a PID library written by Brett Beauregard. A PID system is a control loop feedback mechanism, which continuously measures an error between current state and desired state and adjusts an output parameter accordingly, based upon proportional, integral and derivative constants. Brett Beauregard's function permitted the feeding of a single data parameter, referenced to a constant "set-point", which adjust an output signal. This was edited in such a way that it would take two streams of data, roll and pitch angle, calculate an error with relation to the desired "set-point" roll and pitch angles (controlled and continuously adjusted by the decision system above), which output a signal to the aileron servo and elevator servo.

The accuracy of the system requires optimising, and the three input constants were determined through manual tuning of a mock-system of the Arduino connected to dummy control surfaces. The Ziegler-Nichols method of tuning was attempted but produced dissatisfactory results. Thus, the parameters were adjusted one by one until the system responded quickly and accurately to any perturbation in pitch and roll angle, and the oscillation of output signal critically damped to prevent overshooting of the roll or pitch angle.

The result of which was that for example, were the UAV switched to autopilot at an altitude of 15m, on a bearing of 172, the system would decide that the UAV needed to ascend and turn soft right, adjust the elevator and aileron angle continuously to achieve a roll angle of 5^o and a pitch angle of 13^o until the UAV moved into a different state, where the desired orientation of the UAV was changed accordingly. Once the UAV reached the intended heading and altitude it would fly in a steady level state, with a pitch angle of 3^o determined by the wing design team to give a net vertical force of $0N$.

2.3 Flight Data Recorder

The slave Arduino used the `TinyGPS++` and `SD` libraries, which enabled it to firstly interpret the stream of data from the GPS shield, manipulate it to produce a string every second, which was written to a data file on the microSD card. In addition, the master and slave Arduinos utilised the `Wire` and `SoftwareSerial` libraries to pass information for the data file. The master Arduino already had variables containing control surface angle, pitch angle and roll angle, and these were added to a data string each loop. This was then sent and received character by character to the assigned address of the slave Arduino, which added the data to each line, producing a file containing the data for every second of flight. The parameters included were as follows; latitude, longitude, date and time, velocity, heading, altitude, roll angle, pitch angle, aileron angle, elevator angle. This data would allow us to analyse the performance of the UAV and in particular the autopilot system post-flight.

2.4 High Lift Devices

This was a very simple system of the signal and power from the transmitter AUX1 port being passed to the HLD servos, which deployed the flaps depending upon the position of the flap switch on the transmitter. In addition to this, control of the throttle and rudder were purely manual, the signal being passed at all times from the transmitter to each component, as specified in the design requirements.

2.5 Circuitry

The system was initially produced on a prototype breadboard, and once the design was finalised, it was moved onto permanently soldered strip boards, of which there were four. A strip board was produced for the passing of power from the battery, via the electronic speed controller and receiver to the master Arduino, servos and sensors, in addition to a common ground for the UAV. Secondly a sensor board was produced to place in the nose of the aircraft to prevent any distortion of readings being taken by other electronic components. A relay strip board was produced and a servo connection board was built with headers to allow the fast connection of the servo cables during assembly. Each part was attached to a plywood board with Velcro, with the exception of the sensor board which used cable ties, to ensure the readings were not effected any the movement as allowed by Velcro attachment, and so were permanently positioned with respect to the fuselage during flight.

3 Costing Report

	Activity	Units	No. of units	Price/ Unit	Final Cost	Type
Materials	Floormate-300A Styrofoam	[kg]	0.218	£5.06	£0	Direct
	PLA 3D Printing Filament	[kg]	N/A	£47.00	£0	Direct
	3mm plywood board	[square meters]	0.24	£28.57	£0	Direct
	Servo Motors (included in ARDX kit)	[units]	4	£0	£0	Direct
	Cables for wiring	[metres]	9	£0	£0	Direct
	10mm Diameter, 2mm Thick, Carbon Fibre Tube	[metres]	2	£10.20	£20.40	Direct
	UAV Wing Design Play Pen Microsoft Excel Program for FEA	[No. of Licenses per WD Team member]	1	£0	£0	Direct
	2D & 3D Xfoil CFD Software	[No. of Licenses per WD Team member]	1	£0	£0	Direct
	CAD Software (DS SolidWorks 2017 [Student Edition] & AutoDesk)	[No. of Licenses per group member]	1	£0	£0	Direct
	Flight Computer Sensor Kit (provided)	[No. of Sets of Equipment] *	1	£83.23	£0	Direct
	ARDX Electronics Kit	[No. of Sets of Equipment] **	1	£62.00	£0	Direct
	Flight Computer items provided on flight test day	[No. of Sets of Equipment] ***	1	£229.90	£0	Direct
	Arduino Uno (included in ARDX kit)	[Units]	2	£0	£0	Direct
	Miscellaneous Items	[No. of Sets of Equipment] ****	1	£9.00	£9.00	Indirect
Travel & Subsistence	Travel to and from Flight Testing Site	[No. of Uni-Link Day Tickets]	3	£3.50	£10.50	Direct
Other	Airspace/land for flight testing (Fixed Asset)	[area limit of airspace projected on ground, square meters]	10 000	£0	£0	Indirect
				Total Cost	£39.90	

Figure 3.1: Costing Report

* This set contained... a Spektrum AR610 Receiver (£21.66 cheapest), an ESC, a BMP085 Pressure Sensor (£15.38), an Adafruit Ultimate GPS shield (£34.66 with SD card), and an LSM303DHC Accelerometer & Magnetic sensor (£11.53).
** This set was provided for previous lab classes from semester 1 and contained jumper cables, servos, an Arduino, resistors, relays, diodes etc., so was still useful for this project
*** This set contained... a Spektrum DX8 transmitter (£229.90 cheapest), and the main battery [LiPo]
**** This includes... supplementary items purchased by this group – 60cm Velcro (for £2) duct tape (for £7) - as well as items from the electronics workshop (strip boards, solder) which were free.

Prices quoted for the sensors were obtained from the FEEG2001 blackboard site, using conversion rates valid on 17/05/17, and the prices for the receiver/transmitter were quoted as the cheapest found simply on google.

4 Flight Test Results

4.1 Analysis of Recorded Data

Figure 4.1: The UAV's flight path

As can be seen from the overlay of the GPS path on a satellite map of the testing field, our UAV unfortunately only had a short flight. Nevertheless, the radius of the two controlled turns made proved the agility of the aircraft due to well sized aileron design, and it successfully flew the first lap of the flight testing.

Figure 4.2: Velocity-time plot of the UAV's flight path

In addition, after the UAV was launched from the catapult, it maintained a consistent velocity of around 25-26 knots through the controlled section of the flight (18:08:34 – 18:09:00), as it undertook manoeuvres, indicating the low drag profile of the wing design.

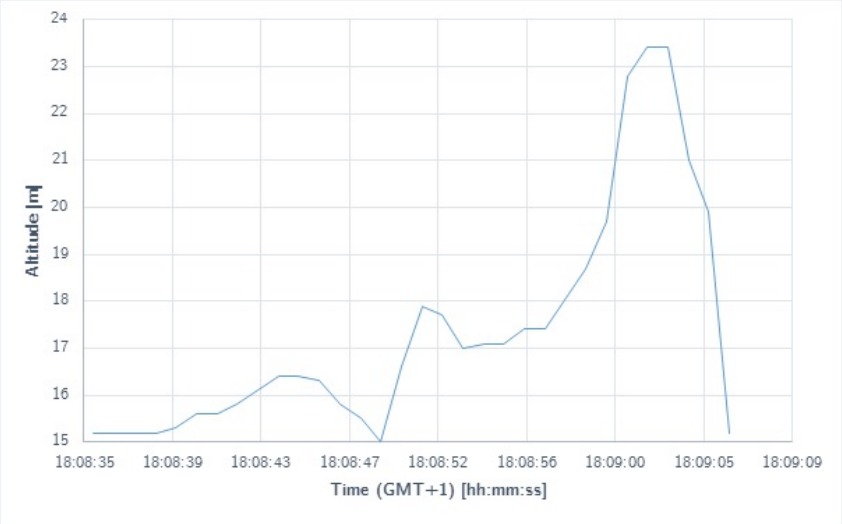

Figure 4.3: Altitude-time plot of the UAV's flight path

The UAV reached a maximum altitude of 23.4m and thus validated the designs of the wings, as it is clear that they produced sufficient lift to enable the aircraft to climb quickly and effectively. In addition, the stability of the aircraft was evidenced by the climb at 18:08:48 where there was little speed change for a fast pull-up manoeuvre. However, what is glaringly obvious is the loss of control of the aircraft at approximately 18:09:00, where the signal from the transmitter to the control surfaces was interrupted, the aircraft continued its increase in pitch rate (as it was climbing slightly at the time of loss of control) as the elevators were stuck at a negative angle of attack, the aircraft stalled, slowing to 8.24 knots, and the UAV nose-dived and crashed into the ground at 18:09:06 at a vertical speed of 4.5m/s and ground speed of 25.7kts. Despite the failure of the control system, the flight data recorder worked superbly throughout. Were the autopilot system able to have been engaged, roll and pitch data, as well as angles for the elevator and aileron angles would have been recorded and would have shown the prowess of the autopilot system. However, some data was collected during the ground testing of the system prior to the flight and produced the following data;

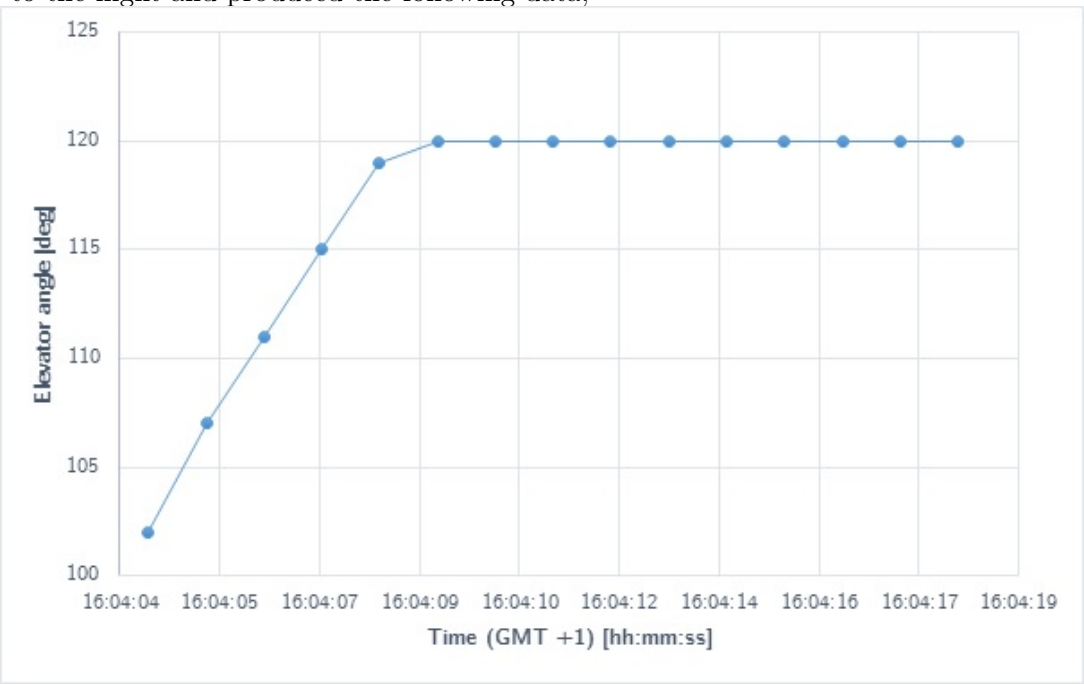

Figure 4.4: Elevator adjustment

Figure 4.4 shows the control of the elevator angle by the autopilot system, when the altitude was below the desired value at a zero pitch angle. Clearly the system reacts quickly to try to pitch the aircraft up by increasing the elevator angle at a high rate to the set maximum limit set of 120^o, as the altitude error is calculated to be 20m. It does not try to overrun this value, nor does it oscillate as the system was critically damped.

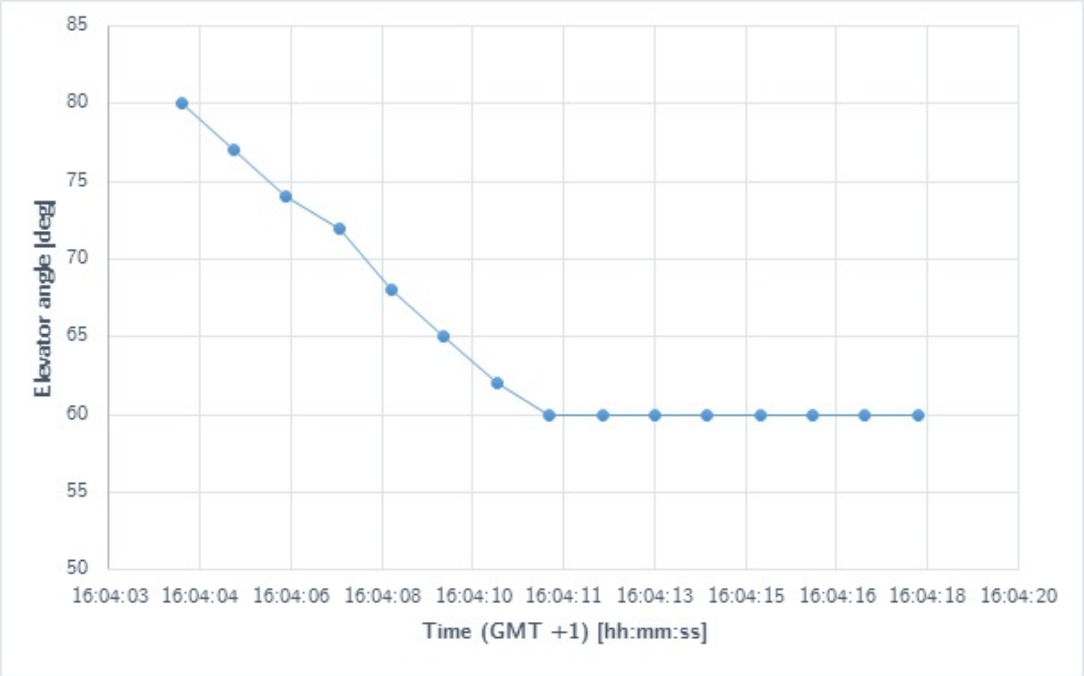

Figure 4.5: Aileron adjustment

In addition, when the data recorded the UAV was on a bearing of 233, and at a roll angle of -6.4^o, the aileron angle was changed in an attempt to roll the aircraft to -10^o. Clearly the error in these values is far less than in the elevator case and so as hoped, the system responds more slowly at a rate of 3.6^o/s, as only a subtle change in roll is required. However, as the aircraft does not react (it is stationary, laid on the ground) the system continues to increase the aileron angle up to the set servo lower limit of 60^o.

This basic analysis of the system, although not indicative of actual flight performance, does show that the system worked, was optimised, and quite obviously had the chance to success as one of the groups key innovations, but was let down by issues with signalling from the transmitter.

4.2 Comments From Pilot

The pilot mentioned the fact that our controls suddenly cut out, which was what had caused the UAV to crash. This was most likely due to faulty electronics (they had been temperamental all afternoon). This was also evident from the fact that the UAV pitched up near the end of the flight, which he later told us he had not commanded. He mentioned the fact that our ailerons were slow to respond and asked about how we were transmitting the signal to the servos operating them. However he then said that this was also probably due to faulty electronics. His final comment was that the ailerons could have been a bit larger, which would have improved the UAV's roll response.

5 Potential Design Improvements

5.1 HLD & Aileron Design

With regards to the HLDs, there are two key areas where the design could be improved. The first was the way in which the servos were attached to the HLDs. The mounts through which the wires were fed were not aerodynamic. This would have increased drag and could have led to adverse yaw effects. This did not seem to be a major problem during the test flight, probably due to the low flight velocity. However if we were to re-design the UAV, we would look to create mounts with smaller aerodynamic cross sections that would lie flat on the HLDs. The second area regards the size of the ailerons. The pilot commented on the fact that they could be slightly larger, which would improve turning speed. We would redo the size optimisation process and try to find a more optimal size. We originally developed smaller ailerons to reduce drag, but if we were to do it again we would take the pilot's advice and worry more about rolling moments than drag reduction.

5.2 Wing Design

The wing seemed to produce sufficient lift for sustained flight and its design was successful. However there were two areas in which the design could be improved. This first is regarding the wing tips of the aircraft. There were no wing tip devices on our wing and its aerofoil cross section extended to the end. This could lead to the formation of vortices at the wing tips, which induces drag. This could be improved through the use of winglets, raked wing tips or some other wing tip devices. This is something that we would consider if we were to redesign the UAV. However due to the fact that the brief limited our wing span, we would need to make the rest of the wing shorter to accommodate the wing. This would have to be taken into consideration, because a shorter wing span will produce less lift. The device that helped hold the wings together could also have been improved. The device was too long and so when we tried moving the wing back to alter the location of the centre of mass, it made contact with the engine and couldn't go further back. If we made the device shorter then we could have moved the wing further back and the centre of mass would have been located at the quarter chord, rather than the third chord at which it was located on our UAV.

5.3 Flight Computer Design

The next step that could be taken to further improve the PID system as described previously would be not to use 15 specific flight states to decide between the desired pitch and roll angle, but to use a calculation that reads the error value in the heading and altitude, and adjusts the desired roll and pitch angle in proportion to that. This calculation in the example of roll could simply be a linear calculation of

$$desiredroll = \frac{headingerror}{180^o}(servolimitangle)$$

Or, for a smoother transition to level flight, but with a higher roll angle at the extremities, a polynomial equation or logarithmic operation on the error/maximum error would produce such a result.

With regard to the flight data recorder, the most effective improvement would be to record data at a higher rate. This would require a completely different GPS encoder and given the memory usage with the current system on the Arduino Uno of 80%, a different microcontroller board would be required. However, the benefit of this would be that the data recorded for the pitch, roll, aileron and elevator angle could be taken at a speed similar to the rate at which these values change, and so a far better judgement on the quality of the system could be made.

Furthermore, clearly improvements are required with regard to the circuitry and transmitter autopilot signal manipulation. The incorrect assumption that the electronics when inserted into the fuselage would not be under such tight constraints meant that the male-female headers, and several soldered wires did not have the structural integrity to withstand the assembly process. An alternative could easily be implemented using headers in which the cable is screwed down rather than soldered, and has a much stronger hold on the cable. This would prevent any future issues with loose cables, a problem we had during the assessment.

In addition, the reading of the gear signal from the receiver was totally inadequate to give a reliable switch between autopilot control and manual control of the UAV. This would require a significant amount of testing to identify the optimal signal pulse length to scan for in the signal, when the switch is active, in order for the relay switch to change in accordance with a single switch on the transmitter, rather than a combination that varied throughout the assessment period.

Nomenclature

Abbreviations

AC	Main wing Aerodynamic Centre
AC_T	Tail-plane Aerodynamic Centre
CG	Wing-Empennage combined Centre of Gravity

Symbols

α	Main wing angle of attack
β	Elevator angle
A	Main wing Aspect Ratio, $A = \frac{b^2}{S}$
A_T	Tail-plane Aspect Ratio, $A_T = \frac{b_T^2}{S_T}$
b	Main wing Span
b_T	Tail-plane Span
c	Main wing Root Chord
$C^*_{L\alpha}$	Partial Derivative of total lift coefficient wrt. α
c_D	Main wing Drag coefficient
c_d	Main wing sectional drag coefficient
C_L	Main wing Lift Coefficient
c_l	Main wing sectional lift coefficient
C^*_L	Total Lift Coefficient of UAV
c_T	Tail-plane chord
$C_{L\alpha}$	Partial Derivative of main wing lift coefficient wrt. α
$C_{LT\alpha}$	Partial Derivative of tail-plane lift coefficient wrt. α
C_{LT}	Tail-plane Lift Coefficient
e	Main wing Oswald span efficiency
e_T	Tail-plane Oswald span efficiency
h	Actual CG position from main wing leading edge (proportion of c)
h_0	AC position from main wing leading edge (proportion of c)
h_n	UAV neutral point position from main wing leading edge (proportion of c)
K	Tail-plane volumetric constant, $K = \frac{S_T l}{Sc}$
l	Distance from main wing leading edge to root-leading-edge of fin
l_0	Distance from AC to AC_T
S	Main wing planform area
S_T	Tail-plane planform area

References

[1] Laurence K. Loftin Jr. *Quest for Performance: The Evolution of Modern Aircraft (NASA SP 468)*. 1985.

[2] Prof. Andy J Keane - University of Southampton. *SESA2023 XFLR5 Stability Analysis*. URL: https://blackboard.soton.ac.uk/webapps/blackboard/execute/content/file?cmd=view&content_id=_3371157_1&course_id=_169526_1&framesetWrapped=true.

[3] Rafic Ajaj - University of Southampton. *SESA2023 Aircraft Static Stability Lecture 1.7. February 2017*. URL: https://blackboard.soton.ac.uk/bbcswebdav/pid-3321226-dt-content-rid-2953811_1/courses/SESA2025-31477-16-17/SESA2025_Lecture_1.7_Lateral.pdf.

Appendices

A Wing Design QFD Tables

Reqts	Weighting	Design Variable					Mapped Importance of Design Variable				
		1	2	3	4	5	1	2	3	4	5
1	0.139	0.9	0.9	0.3	0.9	0.9	0.125	0.125	0.042	0.125	0.125
2	0.194	0.9	0.1	0.9	0.9	0.3	0.175	0.019	0.175	0.175	0.058
3	0.111					0.3	0.000	0.000	0.000	0.000	0.033
4	0.083				0.3		0.000	0.000	0.000	0.025	0.000
5	0.028	0.3		0.9	0.3		0.008	0.000	0.025	0.008	0.000
6	0.167	0.3			0.3		0.050	0.000	0.000	0.050	0.000
7	0.139	0.3		0.3	0.3		0.042	0.000	0.042	0.042	0.000
8	0.139	0.3	0.9		0.3		0.042	0.125	0.000	0.042	0.000
	Absolute Importance						0.442	0.269	0.283	0.467	0.217
	Normalized Importance						0.263	0.161	0.169	0.278	0.129

Figure A.1: QFD analysis of design variables

Reqts	Weighting	Planform Concept					Mapped Importance of Planform Concept				
		1	2	3	4	5	1	2	3	4	5
1	0.139						0.000	0.000	0.000	0.000	0.000
2	0.194	0.9	0.1	0.3	0.3	0.3	0.175	0.019	0.058	0.058	0.058
3	0.111	0.3	0.9	0.9	0.3	0.1	0.033	0.100	0.100	0.033	0.011
4	0.083	0.1	0.9	0.3	0.1	0.1	0.008	0.075	0.025	0.008	0.008
5	0.028		0.3			0.3	0.000	0.008	0.000	0.000	0.008
6	0.167	0.1	0.9	0.9	0.3	0.1	0.017	0.150	0.150	0.050	0.017
7	0.139	0.3	0.9	0.9	0.1	0.1	0.042	0.125	0.125	0.014	0.014
8	0.139						0.000	0.000	0.000	0.000	0.000
	Absolute Importance						0.275	0.478	0.458	0.164	0.117
	Normalized Importance						0.184	0.320	0.307	0.110	0.078

Figure A.2: QFD analysis of planform concepts

Reqts	Weighting	Manufacture Method		Mapped Importance of Manufacture Method	
		1	2	1	2
1	0.139	0.3	0.9	0.042	0.125
2	0.194	0.3	0.3	0.058	0.058
3	0.111	0.9	0.3	0.100	0.033
4	0.083	0.9	0.3	0.075	0.025
5	0.028	0.9	0.9	0.025	0.025
6	0.167	0.9	0.3	0.150	0.050
7	0.139	0.3	0.9	0.042	0.125
8	0.139			0.000	0.000
	Absolute Importance			0.492	0.442
	Normalized Importance			0.527	0.473

Figure A.3: QFD analysis of manufacturing methods

B Wing Planform Optimisation

USER INPUTS

Geometric Inputs	Lower Bounds		Upper Bounds	Units
Semi-Span	0.6	0.6	0.9	m
Root Chord	0.15	0.15	0.25	m
Taper Ratio	0.6	0.6	1	-
Max. Airfoil t/c	0.15	0.15	0.25	-

Flight Inputs				Units
Altitude	-	100	-	m
Velocity	-	12.5	-	m/s

Weigth Inputs				Units
Wing Mass	-	0.2397	-	kg
Fuselage (and all else) Mass	-	0.766	-	kg

Additional Inputs				Units
Oswald (Span) Efficiency	-	0.8	-	-
Maximum Load Factor	-	7	-	g

PROGRAM OUTPUTS

Calc. Geo. Properties		Upper Limit	Units
Wing Area	0.144	-	m^2
Aspect Ratio	10	-	-

Calc. Flig. Properties			Units
Density at Alt.	1.213290238	-	kg/m^3
Dyn. Visc. At Alt	1.77998E-05	-	kg/ms

Calc. Flig. Properties			Units
Reynolds Number	102244.5577	-	-
Coefficient of Lift	0.722803475	-	-

Calc. Perf. Properties			Units
Induced Drag Coef., CDi	0.020787421	-	-
Profile Drag Coef., CDp	0.012997683	-	-
Total Drag Coef., CD	**0.033785104**	-	-
Total Drag	0.461150285	-	N
Cruise Wing Load.	68.5133125	35	N/m^2
Max Root BM. at Load Factor	3.557155859	-	Nm

Figure B.1: Starting parameters used in Wing Design Play-Pen Aerodynamics spreadsheet

USER INPUTS

Geometric Inputs	Lower Bounds		Upper Bounds	Units
Semi-Span	0.6	0.6	0.9	m
Root Chord	0.15	0.15	0.25	m
Taper Ratio	0.6	0.6	1	-
Max. Airfoil t/c	0.15	0.15	0.25	-
Location of Max. t/c	-	0.25	-	-

Spar Inputs				Units
Spar Type		Circ. Spar		-
Spar Thickness	-	0.001	-	m
Spar Ext. Diam.	-	0.01	-	m
-	-	-	-	-

Aero. Inputs				Units
Max Root BM. at Load Factor	-	3.557156	-	Nm

Material Properties				Units
Spar Density	-	1700	-	kg/m^3
Foam Density	-	36	-	kg/m^3

Aux. Wing Masses	-			Units
Mass of single Servos	-	0.020	-	kg
Number of Servos	-	6	-	-
Auxiliary Masses	-	0.000	-	kg

PROGRAM OUTPUTS

Calc. Spar Properties	Lower Limit		Upper Limit	Units
Outer Rad.	-	0.0050	-	m
Inner Rad.	-	0.0040	-	m
-	-	-	-	m
-	-	-	-	m
Dist. from Neut. Axis	-	0.0050	-	m
Second Mom. Area	-	2.898E-10	-	m^4
Cross Sec. Area	-	2.827E-05	-	m^2
Semi Spar Volume	-	1.696E-05	-	m^3

Calc. Load Properties				Units
Axial Str. from Bend.	-	6.137E+07	5.00E+08	Pa

Calc. Geom. Properties				Units
Cut-out Fraction	-	0.7	-	-
Foam Section Root Area	-	0.0022358	-	m^2
Foam Section Tip Area	-	0.0008049	-	m^2
Tot. Spar Clearance (at Tip)	0.02	0.0035	-	m

Calc. Wing Masses				Units
Total Foam Sect. Mass	-	0.062022	-	kg
Total Mass Spar	-	0.0577	-	kg
Total Aux Masses	-	0.1200	-	kg
Total Wing Mass	-	**0.2397**	-	kg

Figure B.2: Starting parameters used in Wing Design Play-Pen Structures spreadsheet

C Aerofoil Optimisation

```
load file_path\aerofoil.dat
panel
oper
visc 856164.3836
M 0.03673337447
type 1
pacc
file_path\polar.dat

iter
5000
cl 0.364


quit
```

Figure C.1: Commands used for the aerofoil analysis in XFoil 6.99

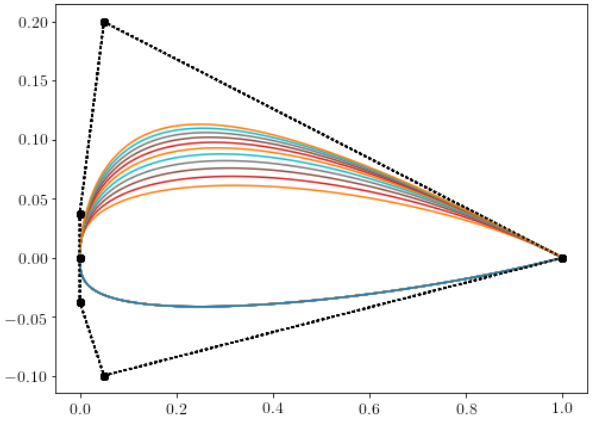

Figure C.2: Plot of the Bezier aerofoil, varying the upper control point weighting (lowerweight=0.5)

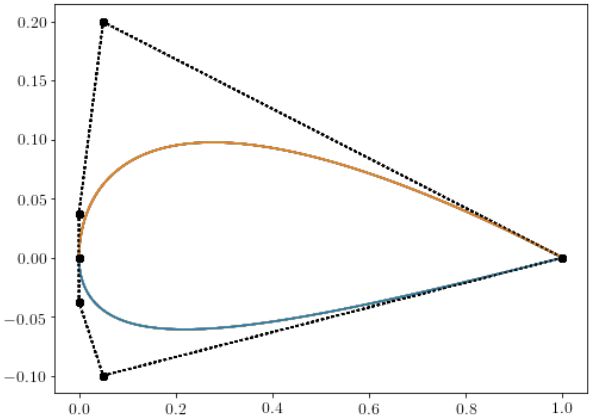

Figure C.3: Aerofoil 5

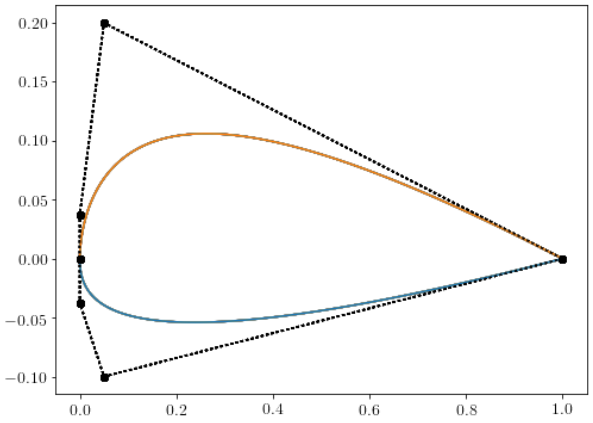

Figure C.4: Aerofoil 6

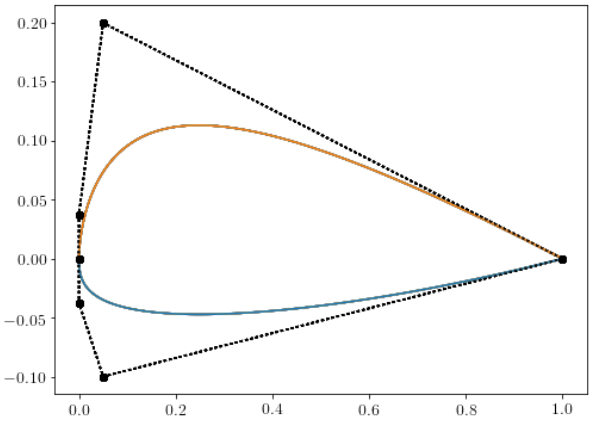

Figure C.5: Aerofoil 7

D HLD & Aileron Optimisation

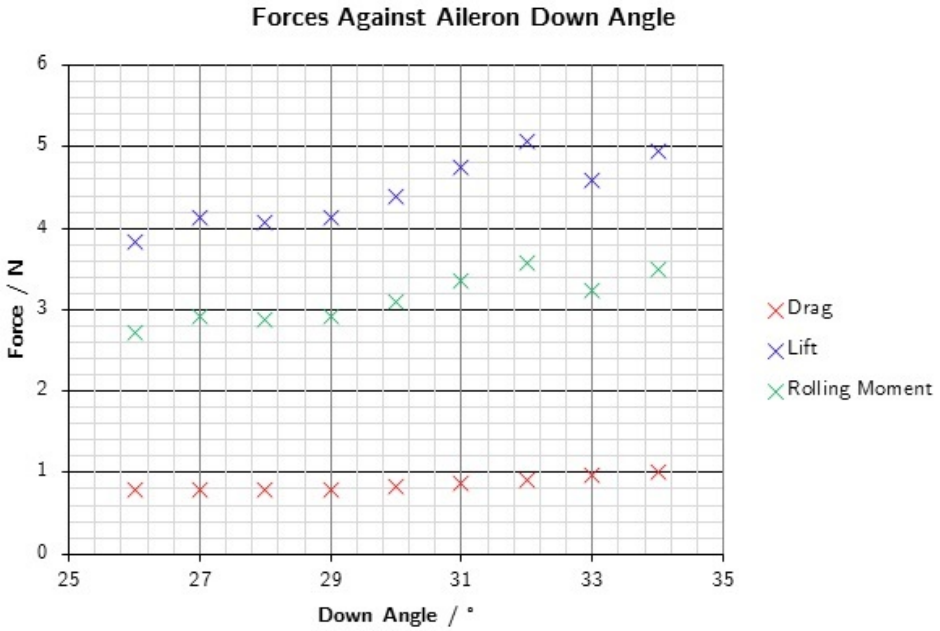

Figure D.1: A plot of the results of SolidWorks simulations to find the optimum down angle of aileron

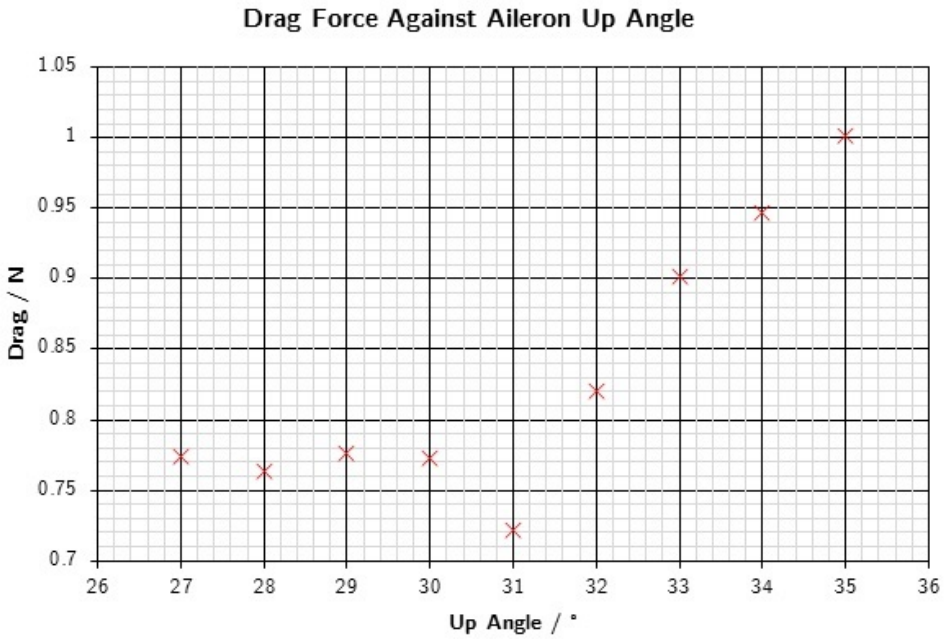

Figure D.2: A plot of the drag against aileron up angle as a result of SolidWorks simulations

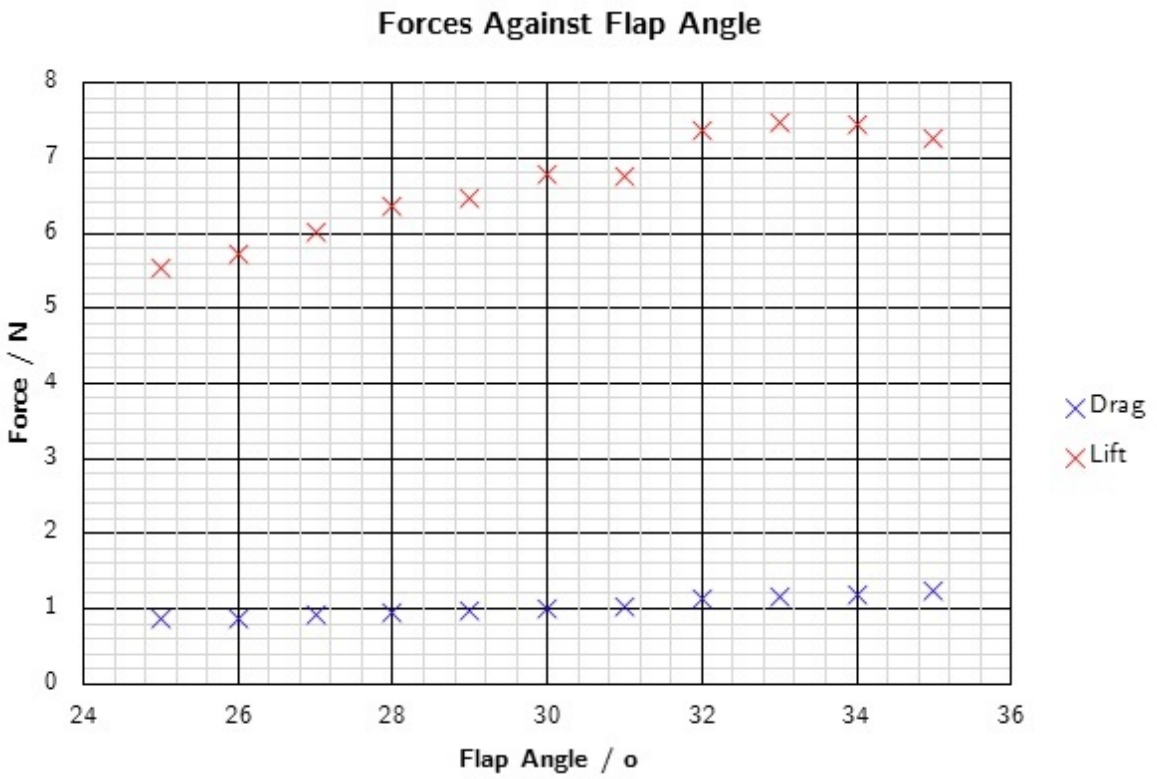

Figure D.3: A plot of the flap deployment angle against the lift and drag force produced by one wing